Spin and Fluorescent Probing of the Binding Interface between Tissue Factor and Factor VIIa at Multiple Sites

Rikard Owenius,* Maria Österlund,† Magdalena Svensson,† Mikael Lindgren,* Egon Persson,‡ Per-Ola Freskgård,§ and Uno Carlsson†

*IFM-Department of Chemical Physics and †IFM-Department of Chemistry, Linköping University, SE-581 83 Linköping, Sweden; ‡Department of Vascular Biochemistry, Novo Nordisk A/S, DK-2760 Måløv, Denmark; and §Department of Protein Biotechnology, Novo Nordisk A/S, DK-2880 Bagsværd, Denmark

ABSTRACT The specific complex between the extracellular part of tissue factor (sTF) and factor VIIa (FVIIa) was chosen as a model for studies of the binding interface between two interacting proteins. Six surface-exposed positions in sTF, residues known to contribute to the sTF-FVIIa interaction, were selected for cysteine mutation and site-directed labeling with spin and fluorescent probes. The binding interface was characterized by spectral data from electron paramagnetic resonance (EPR) and steady-state and time-domain fluorescence spectroscopy. The labels reported on compact local environments at positions 158 and 207 in the interface region between sTF and the γ-carboxyglutamic acid (Gla) domain of FVIIa, and at positions 22 and 140 in the interface region between sTF and the first epidermal growth factor-like (EGF1) domain of FVIIa. The tightness of the local interactions in these parts of the interface is similar to that seen in the interior of globular proteins. This was further emphasized by the reduced local polarity detected by the fluorescent label upon FVIIa binding, especially in the sTF-Gla region. There were indications of structural rigidity also at positions 45 and 94 in the interface region between sTF and the protease domain (PD) of FVIIa, despite the perturbed cofactor function of these sTF variants. The results of the present study indicate that the multi-probing approach enables comparison of the tightness and characteristics of interaction along the binding interface of a protein complex. This approach also increases the probability of acquiring reliable structural data that are descriptive of the wild-type proteins.

INTRODUCTION

Many biologically important processes in the body, such as cell signaling, transcription, immunity, and transport are dependent on, and regulated by, the formation of highly specific, non-covalent complexes between proteins. The physiological relevance of these protein-protein interactions has drawn the attention to questions concerning protein recognition, specificity, association kinetics, and the connection between binding affinity and biological activity. Protein-protein interactions are governed by the chemical properties, shape, and flexibility of the encountering molecules.

We have chosen the extracellular domain of tissue factor (sTF, i.e., soluble TF) and the activated form of factor VII (FVIIa) as a model system. In vivo, the binding of FVIIa to membrane-anchored TF is the primary event in the coagulation cascade. sTF is a 219-residue protein composed of two immunoglobulin-like domains, and its crystal structure has been solved (Harlos et al., 1994; Muller et al., 1994, 1996). FVIIa consists of 406 residues that are divided into four domains: a catalytic serine protease domain (PD), two epidermal growth factor-like domains (EGF1, EGF2), and a γ-carboxyglutamic acid (Gla) domain. The complex formation between sTF and FVIIa (sTF-FVIIa) involves all sTF and FVIIa domains (Fig. 1), creating an extended contact area, which is a common feature of heterodimeric complexes (Lo Conte et al., 1999). This area is divided into three regions: sTF-PD, sTF-EGF1, and sTF-Gla (Banner et al., 1996). The sTF structure is unaltered by the binding of FVIIa. The solved crystal structure of sTF-FVIIa (Banner et al., 1996) and mutational studies of sTF (Gibbs et al., 1994; Ruf et al., 1994, 1995; Schullek et al., 1994; Kelley et al., 1995) have resulted in a detailed picture of the residues in sTF that are most important for the binding of FVIIa.

The objective of this study was to further investigate the local environmental properties of the binding interface of the sTF-FVIIa complex. The interaction between sTF and FVIIa was studied at six selected positions in sTF: I22, W45, Y94, F140, W158, and V207. All of them are located on the surface of sTF, with a surface accessibility of 18–62% according to the crystal structure (Muller et al., 1996), and they are distributed over the three binding regions (Fig. 1). W158 and V207 are located in the sTF-Gla region and I22 and F140 are situated in the sTF-EGF1 region, whereas W45 and Y94 reside in the sTF-PD region. Four of the six chosen positions, I22, W45, Y94, and F140, were previously defined to make moderate to large contributions to the affinity of sTF for FVIIa binding, whereas W158 and V207 were found to have a role in the coagulant function of sTF, but not in FVIIa binding (Kelley et al., 1995). However, it is known from the crystal structure of sTF-FVIIa that W158

Received for publication 13 April 2001 and in final form 6 July 2001.

Address reprint requests to Dr. Uno Carlsson, IFM-Department of Chemistry, Linköping University, SE-581 83 Linköping, Sweden. Tel.: +46-1328-1714; Fax: +46-1328-1399; E-mail: ucn@ifm.liu.se.

Mikael Lindgren's present address is Department of Laser Systems, Swedish Defense Research Agency, P.O. Box 1165, SE-581 11 Linköping, Sweden.

Per-Ola Freskgård's present address is Maxygen ApS, Agern Alle 1, DK-2970 Hørsholm, Denmark.

0006-3495/01/10/2357/13 $2.00

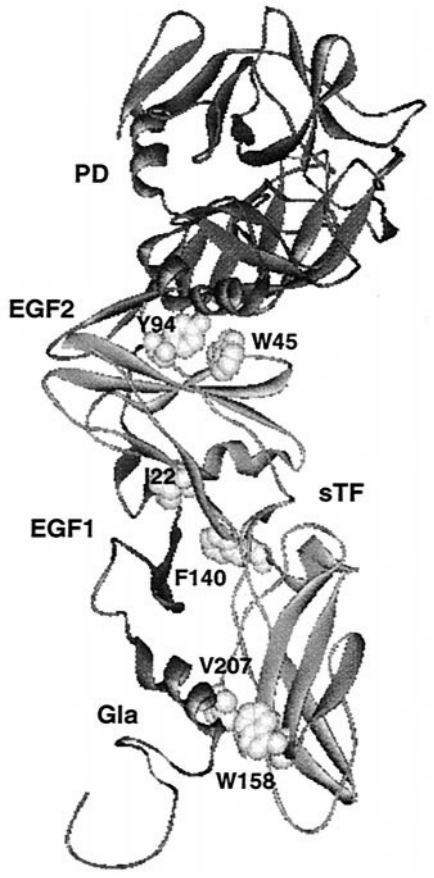

FIGURE 1 The crystal structure of the sTF-FVIIa complex. sTF is shown in light gray and the four domains of FVIIa (Gla, EGF1, EGF2, and PD) in dark gray. The six positions in sTF selected for Cys mutation and labeling are shown in white (displayed as space-filling models). W158 and V207 are located in the sTF-Gla region, I22 and F140 in the sTF-EGF1 region, and W45 and Y94 in the sTF-PD region. The figure was generated using the program WebLab ViewerLite 3.10 (Molecular Simulations Inc., San Diego, CA) and the coordinates from Banner et al., 1996.

and V207 take part in major hydrophobic interactions between sTF and FVIIa (Banner et al., 1996).

The methodological approach of site-directed labeling was used, which involves specific attachment of various reporter groups such as spin or fluorescent labels. Local structural information about the protein(s) of interest can then be obtained via electron paramagnetic resonance (EPR) or fluorescence spectroscopy measurements (Berliner and Reuben, 1989; Likhtenshtein, 1993; Carlsson and Jonsson, 1995; Hubbell et al., 1996, 1998, 2000; Feix and Klug, 1998; Lakowicz, 1999). First, we performed single-Cys mutations at the selected six positions in sTF, where the Cys residue constitutes the handle for the reporter groups. Then, the Cys mutants were labeled with two different spin labels (IPSL and MTSSL) and one fluorescent label (IAEDANS). The lineshapes of the 9-GHz EPR spectra were simulated and analyzed in terms of local (internal) motion of the spin label and global (overall) motion of the protein. The fluorescence wavelength, quenching, anisotropy, and lifetime data provided additional information on label dynamics and environmental properties in the vicinity of the label. Recently, the site-directed labeling approach was used on the sTF-FVIIa complex (position F140 in sTF) to evaluate the applicability of the method, the performance of different labels, and the influence of Ca^{2+} and the Gla domain on the sTF-EGF1 interaction (Owenius et al., 1999; Österlund et al., 2000). In this study we combine information on the dynamics of the labels with physicochemical data of their immediate environment to analyze and compare the characteristics of the three regions of the sTF-FVIIa binding interface. We also discuss the influence of mutation- and labeling-induced structural and functional perturbations on the EPR and fluorescence data, and point at benefits of using a multi-probing approach.

MATERIALS AND METHODS

Chemicals

The spin label *N*-(1-oxyl-2,2,5,5-tetramethyl-3-pyrrolidinyl)iodoacetamide (IPSL) was purchased from Sigma, Stockholm, Sweden and the spin label (1-oxyl-2,2,5,5-tetramethylpyrroline-3-methyl)methanethiosulfonate (MTSSL) was obtained from Reanal, Budapest, Hungary. The fluorescent label 5-((((2-iodoacetyl)amino)ethyl)amino)naphthalene-1-sulfonic acid (1,5-IAEDANS) was obtained from Molecular Probes, Eugene, OR. All other chemicals used were of analytical grade.

Protein isolation, purification, and labeling

The single-Cys mutants of sTF, with the substitutions I22C, W45C, Y94C, F140C, W158C, and V207C, were expressed in *Escherichia coli* and purified by Q Sepharose and FVIIa affinity chromatography as described earlier (Owenius et al., 1999). The isolation of human recombinant FVIIa and preparation of the FVIIa affinity matrix have been described elsewhere (Thim et al., 1988; Freskgård et al., 1996). Protein concentrations were determined on a Hitachi U-2000 spectrophotometer. The attachment of spectroscopic labels to the free Cys residue of the various sTF mutants was performed as previously described (Owenius et al., 1999). A final purification step was performed after labeling using FVIIa affinity chromatography.

Activity measurements

An amidolytic assay was performed to determine the cofactor activity of the unlabeled and labeled sTF mutants, as described in Persson et al. (1997). Briefly, the cofactor function of the sTF variants was assessed by measuring the amidolytic activity of 10 nM FVIIa in the presence of various concentrations of sTF variant (0–500 nM) in 50 mM Hepes, 150 mM NaCl, 5 mM $CaCl_2$, pH 7.5. The maximal activity was compared to that of the wild-type FVIIa-sTF complex (set to 100%) and $K_{d(app)}$ is the concentration of sTF variant giving half-maximal activity.

EPR measurements

EPR measurements were carried out using a Bruker CW X-band spectrometer consisting of a combination of the ER200D-SRC and ESP300 systems. An ER4103TM cavity was connected to the 200 mW microwave bridge. The different protein samples were introduced in a standard TM_{110} flat cell

for aqueous samples (Wilmad Glass, Buena, NJ). Two sets of samples were prepared: 1) the six sTF mutants labeled with either IPSL or MTSSL in 50 mM Hepes, 150 mM NaCl, pH 7.5; and 2) FVIIa in a 1.5-fold molar excess over sTF together with the six IPSL- or MTSSL-labeled sTF mutants in 50 mM Hepes, 150 mM NaCl, pH 7.5, with $CaCl_2$ added to a final concentration of 5 mM. The sTF concentration was 6–11 μM in all samples. EPR spectra were acquired at 20 ± 1°C using 400 μl sample volume. The modulation amplitude was set lower than one-half (sTF) or one-third (sTF-FVIIa) of the linewidth of the $m_I = 0$ nitrogen hyperfine transition and the microwave power was set to 4 mW.

EPR lineshape simulations

To analyze X-band EPR spectra and estimate the dynamic parameters of the spin labels in the various locations in sTF and at the binding interface between sTF and FVIIa, the program "nlslpl" developed by Freed and co-workers was used (Budil et al., 1996). This program makes it possible to perform nonlinear least-squares analysis of EPR spectra in the slow-motional regime (Freed, 1976).

The same hyperfine coupling (A) tensor and g tensor components for IPSL and MTSSL were used as in Owenius et al. (1999). Different A_{zz} components were used in simulations of labeled sTF spectra than in simulations of labeled sTF-FVIIa spectra, because the polarity of the environment of the spin label was known to decrease upon FVIIa-binding to sTF. A decreased polarity has been found to result in a decreased A_{zz} (Krinichnyi et al., 1985; Ondar et al., 1985), as well as a concomitant increase in g_{xx}. However, the changes in g_{xx} were found to be insignificant in our simulations.

In simulations of spectra from spin-labeled sTF, the A_{zz} of a solvent-exposed spin label was used. One axially symmetric motional component was assumed, with Brownian diffusion tensor [$R_\perp$, $R_\parallel$], whose frame of rotation is related to the magnetic frame through the diffusion tilt angle (β) (see Fig. 2 in Schneider and Freed, 1989). A second axially symmetric motional component with the same A_{zz} (but with different local dynamics) was included in the simulations in cases where the spectral lineshape indicated two components. The two-component spectra correspond to two populations of spin labels experiencing different local environments. In simulations of spectra from spin-labeled sTF in complex with FVIIa, i.e., in the case of spectra with near-rigid limit features, the A_{zz} of a buried spin label was used. The Brownian diffusion tensor was assumed to be isotropic ($R = R_\perp = R_\parallel$, $\beta = 0°$). This component represents a motional range from the global (overall) motion of the protein complex (due to a tightly locked spin label) to minor local motion of the spin label. Also here, a second motional component, axially symmetric with the A_{zz} of a solvent-exposed spin label, was added if there were signs of fast local spin-label motion in the spectra.

In all simulations the A- and g-tensor components were defined as constants, whereas $R_\perp$, $R_\parallel$ (or R), β (except for isotropic motion), and the Gaussian linewidth (gw) of each defined motional component were varied from their start values in the iterative nonlinear least-squares fit of the experimental spectrum, until a satisfactorily good fit was obtained. When two spectral components were defined, the relative contribution (c_r) of each component was given. To reduce the number of parameters in the fit the Lorentzian linewidth tensor [lw_{xx}, lw_{yy}, lw_{zz}] was not specified. As in Owenius et al. (1999) the estimated errors for A_{ii} and g_{ii} were ±0.2 G and ±0.0002, respectively.

The rotational correlation time (ϕ_c) of a specific motional component was determined from the Brownian diffusion tensor according to

$$\phi_c = \frac{1}{6R} = \frac{1}{6\sqrt{R_\perp R_\parallel}} \quad (1)$$

(Goldman et al., 1972).

Steady-state fluorescence measurements

Fluorescence measurements at equilibrium conditions were performed on a Hitachi F-4500 spectrofluorimeter equipped with a thermostatic sample compartment unit holding a magnetic stirrer. Emission spectra were registered from each of the IAEDANS-labeled sTF mutants, [sTF] = 1 μM, in 50 mM Hepes, 150 mM NaCl, pH 7.5. After addition of FVIIa in 1.5-fold molar excess over sTF and $CaCl_2$ to a final concentration of 5 mM, another set of spectra was recorded. The excitation wavelength was 350 nm and the emitted light was collected in the region 400–600 nm. The wavelength shift ($\Delta\lambda_{Fmax}$) was defined as the difference between the wavelengths of the emission intensity maxima of sTF-FVIIa and sTF, i.e., $\Delta\lambda_{Fmax} = \lambda_{Fmax}$(sTF-FVIIa) − λ_{Fmax}(sTF).

The same samples were used for subsequent acrylamide quenching of the fluorescence. The IAEDANS-fluorescence was quenched by progressive addition of 2.5 μl aliquots of 5.6 M acrylamide solution every 8 s by an automatic Microlab 1000 burette to the cuvette (Hamilton Bonaduz AG, Bonaduz, Switzerland). After excitation of the IAEDANS molecule at 350 nm the quenched fluorescence was monitored at the emission maximum of the respective sTF or sTF-FVIIa sample. Fluorescence registration was continued to a final acrylamide concentration of 600 mM during continuous stirring. Quenching data were analyzed according to the modified Stern-Volmer equation,

$$\frac{F_0}{\Delta F} = \frac{1}{f_a K_{SV,a}[Q]} + \frac{1}{f_a} \quad (2)$$

assuming that there are two populations of fluorophores, one accessible to the quencher (a) and the other inaccessible or buried. F_0 is the total fluorescence (intensity) in the absence of quencher and $\Delta F = F_0 - F$, where F is the measured fluorescence at quencher concentration [Q]. f_a is the fraction of the initial fluorescence that is accessible to the quencher and $K_{SV,a}$ is the Stern-Volmer constant of the accessible fraction. f_a and $K_{SV,a}$ were determined graphically from modified Stern-Volmer plots for each sample (Lakowicz, 1999).

Fluorescence anisotropy spectra were recorded for the same samples. The polarization of the excited and emitted light was changed between vertical (v) and horizontal (h). The emitted fluorescent light for IAEDANS was collected in the range 400–600 nm. The fluorescence anisotropy (r_s) was calculated over the wavelength interval using the conventional formula:

$$r_s(\lambda) = \frac{F_{vv}(\lambda) - G(\lambda)F_{vh}(\lambda)}{F_{vv}(\lambda) + 2G(\lambda)F_{vh}(\lambda)} \quad (3)$$

where F_{vv} and F_{vh} are the fluorescence intensities at a given wavelength with the respective polarization configuration. G is an apparatus constant taking into account the polarization dependence of the detection system, $G(\lambda) = F_{hv}(\lambda)/F_{hh}(\lambda)$. The final r_s value was then determined as the average r_s over the given wavelength interval.

All measurements were performed with the samples in a 1-cm quartz cell maintained at 23°C with a 5-nm bandwidth for both excitation and emission.

Time-resolved fluorescence measurements

Fluorescence lifetimes of the IAEDANS-labeled sTF mutants in absence and presence of FVIIa were measured using a miniature fluorescence lifetime analyzer, mini-τ (Edinburgh Instruments Ltd., Edinburgh, UK) equipped with a PDL 800-B pulsed diode laser (PicoQuant GmbH, Berlin, Germany). Measurements were made at room temperature (21 ± 1°C), using 380 nm excitation pulses (10 MHz repetition rate, ~500 ps pulse width). The emission was monitored through a FCG065 long pass filter (>475 nm) (Melles Griot, Inc., Irvine, CA). The Brewster angle polarizers were set in "magic angle" configuration, i.e., the analyzer polarizer was set

TABLE 1 Functional binding of unlabeled and labeled sTF variants to FVIIa as measured by amidolytic activity stimulation

sTF Variant*	$K_{d(app)}$† (nM)			
	Unlabeled	IPSL	MTSSL	IAEDANS
W158C	13	4.8	3.8	9.5
V207C	22	9.6	3.9	13
I22C	26	20	27	66
F140C‡	60	110	27	40
W45C	300	1600	440	230
Y94C	21	99	1300	130

*W158 and V207 in the sTF-Gla region, I22 and F140 in the sTF-EGF1 region, and W45 and Y94 in the sTF-PD region.
†$K_{d(app)}$ for wt-sTF is 2.0 nM (Österlund et al., 2000).
‡$K_{d(app)}$ values for derivatives of sTF(F140C) are taken from Österlund et al. (2000).

54.7° with respect to the excitation polarization. The emitted photons were detected with a Pentium-II PC-based SPC-300 single photon counter (v. 5.2) with a 12-bit ADC (Edinburgh Instruments Ltd./PicoQuant GmbH) and were collected in 4096 channels. A 1-cm quartz cell was used and the measurement time was 20 min. The instrument response function (IRF) was determined by measuring light scatter from a turbid reference solution. In this way, adjustment for the lifetime of the excitation could be made. Data were analyzed using the F900 (v. 5.13) analysis toolkit (Edinburgh Instruments Ltd.). A single-exponential decay function was fitted to each experimental data set using both a reconvolution fit method and tail fit method yielding essentially the same results, as the lifetimes of IAEDANS generally were longer than the excitation lifetime.

From the anisotropy (r_s) and lifetime (τ) of the fluorophore the rotational correlation time (ϕ_c) was calculated from the Perrin equation,

$$r_s = \frac{r_0}{1 + \tau/\phi_c} \quad (4)$$

assuming r_0 to be 0.4 for IAEDANS

RESULTS

Functional characterization of the sTF variants

The protease activity of FVIIa is enhanced by the allosteric changes that take place upon complex formation with sTF. The ability of the sTF variants to stimulate FVIIa activation, i.e., the cofactor function, was assessed using an amidolytic assay. The allosteric enhancement of the amidolytic activity of FVIIa critically depends on a proper binding between sTF and FVIIa. In Table 1 the functional $K_{d(app)}$ values obtained for the unlabeled and labeled sTF variants are shown, reflecting the affinities of the variants for FVIIa. As expected, replacement of the wild-type residue (Trp, Val, Ile, Phe, or Tyr) with a Cys increased the $K_{d(app)}$ for each of the studied positions compared with wild-type sTF (wt-sTF).

The surface accessibility of the wt-sTF residues (Table 2) made it possible to achieve almost complete labeling of the introduced Cys residue with all of the labels. Attachment of labels to the mutated sites had various additional effects on the affinity for FVIIa (Table 1). Linking a label to sTF(W158C) and sTF(V207C) (sTF-Gla region) resulted overall in decreased $K_{d(app)}$ values, making the variants functionally more similar to wt-sTF. The labeled variants of sTF(I22C) and sTF(F140C) (sTF-EGF1 region) resulted in either decreased or increased $K_{d(app)}$ values depending on label used, whereas those of sTF(W45C) and sTF(Y94C) (sTF-PD region) showed almost exclusively increased $K_{d(app)}$ values. Despite the sometimes large functional perturbation, the formation of the sTF-FVIIa complex was promoted by using relatively high protein concentrations (see Materials and Methods).

Probing the attachment sites in sTF in the absence of FVIIa

In the absence of FVIIa, the six selected residues in sTF are surface-exposed to 18–62% (Table 2) in the crystal structure (Muller et al., 1996). The mutation and labeling result in new side chains, and thereby altered degrees of surface accessibility. Fluorescence acrylamide quenching experiments were performed to determine the exposure of the dansyl fluorophore of the IAEDANS side chain, located ~11 Å from the C_α of the backbone (Hammarström et al., 2001), when attached to the sTF mutants. We found that the Stern-Volmer plots displayed curvatures characteristic of

TABLE 2 Fluorescence parameters obtained from steady-state experiments of IAEDANS-labeled sTF mutants

sTF Variant*	$\Delta\lambda_{Fmax}$† (nm)	λ_{Fmax} (nm)	$K_{SV,a}$ (M^{-1})		SA‡ (%)
		sTF-FVIIa	sTF	sTF-FVIIa	wt-sTF/wt-sTF-FVIIa
W158C	−15	477	4.5	0.5	18/5
V207C	−30	465	4.3	1.4	45/0
I22C	−5	490	3.4	2.4	30/5
F140C	−10	487	5.6	1.8	62/20
W45C	−1	489	4.5	2.9	25/13
Y94C	−2	490	5.6	3.7	45/1

*W158 and V207 in the sTF-Gla region, I22 and F140 in the sTF-EGF1 region, and W45 and Y94 in the sTF-PD region.
†$\Delta\lambda_{Fmax} = \lambda_{Fmax}$(sTF-FVIIa) − λ_{Fmax}(sTF).
‡Surface accessibility (*SA*) values (relative the total surface area of the residue) were calculated from the solved crystal structures of wt-sTF (Muller et al., 1996) and wt-sTF-FVIIa (Banner et al., 1996) using the Sybyl 6.3 software (Tripos Inc., St. Louis, MO) on a Silicon Graphics work station.

TABLE 3 EPR parameters of IPSL and MTSSL attached to different sTF mutants in the absence of and in complex with FVIIa, obtained from lineshape simulations of EPR spectra

		sTF			sTF-FVIIa			
		IPSL‡	MTSSL§		IPSL‡		MTSSL§	
sTF Variant*	Parameter†	c_1	c_1	c_2	Slow	Fast	Slow	Fast
W158C	$R_\perp$ (s^{-1})	3.1×10^7	2.6×10^7	1.9×10^7	1.4×10^7	—	1.1×10^7	—
	$R_\parallel$ (s^{-1})	8.4×10^8	2.6×10^7	6.5×10^8	1.4×10^7	—	1.1×10^7	—
	β (°)	25	0	39	0	—	0	—
	c_r (%)	100	66	34	100	—	100	—
V207C	$R_\perp$ (s^{-1})	2.8×10^7	2.5×10^7	5.4×10^7	1.4×10^7	—	5.7×10^6	—
	$R_\parallel$ (s^{-1})	1.2×10^9	2.5×10^7	3.6×10^9	1.4×10^7	—	5.7×10^6	—
	β (°)	34	0	31	0	—	0	—
	c_r (%)	100	74	26	100	—	100	—
I22C	$R_\perp$ (s^{-1})	2.4×10^7	5.2×10^6	—	7.0×10^6	—	1.9×10^6	—
	$R_\parallel$ (s^{-1})	6.6×10^8	1.1×10^8	—	7.0×10^6	—	1.9×10^6	—
	β (°)	34	47	—	0	—	0	—
	c_r (%)	100	100	—	100	—	100	—
F140C	$R_\perp$ (s^{-1})	3.1×10^7	1.3×10^7	—	1.2×10^7	2.0×10^7	2.0×10^6	—
	$R_\parallel$ (s^{-1})	9.2×10^8	3.5×10^8	—	1.2×10^7	7.6×10^8	2.0×10^6	—
	β (°)	36	36	—	0	33	0	—
	c_r (%)	100	100	—	63	37	100	—
W45C	$R_\perp$ (s^{-1})	3.6×10^7	7.2×10^6	—	3.1×10^7	3.5×10^7	2.0×10^6	2.9×10^7
	$R_\parallel$ (s^{-1})	8.2×10^8	3.4×10^8	—	3.1×10^7	1.4×10^9	2.0×10^6	1.0×10^9
	β (°)	40	44	—	0	35	0	23
	c_r (%)	100	100	—	50	50	46	54
Y94C	$R_\perp$ (s^{-1})	3.8×10^7	1.8×10^7	1.7×10^7	3.2×10^6	2.7×10^7	1.4×10^7	1.6×10^7
	$R_\parallel$ (s^{-1})	1.7×10^9	3.5×10^8	5.2×10^8	3.2×10^6	1.5×10^9	1.4×10^7	4.0×10^8
	β (°)	32	28	44	0	35	0	33
	c_r (%)	100	74	26	26	74	26	74

*W158 and V207 in the sTF-Gla region, I22 and F140 in the sTF-EGF1 region, and W45 and Y94 in the sTF-PD region.
†Parameters are defined in Materials and Methods.
‡EPR*g*- and hyperfine tensor components used in simulations of IPSL spectra: $g_{xx} = 2.0084$, $g_{yy} = 2.0056$, $g_{zz} = 2.0022$, $A_{xx} = 6.5$ G, $A_{yy} = 5.5$ G, $A_{zz} = 35.0$ G (slow), $A_{zz} = 35.9$ G (c_1, fast) (Owenius et al., 1999). Gaussian linewidths: (sTF) 1.0–1.4 G; (sTF-FVIIa) 1.5–3.7 G (slow), 1.5 G (fast).
§EPR- and hyperfine tensor components used in simulations of MTSSL spectra: $g_{xx} = 2.0080$, $g_{yy} = 2.0059$, $g_{zz} = 2.0023$, $A_{xx} = 7.1$ G, $A_{yy} = 6.0$ G, $A_{zz} = 34.7$ G (slow), $A_{zz} = 35.5$ G (c_1, c_2, fast) (Owenius et al., 1999). Gaussian linewidths: (sTF) 0.6–2.8 G (c_1), 1.3–2.0 G (c_2); (sTF-FVIIa) 0–4.2 G (slow), 0.5–1.7 (fast).

two fluorophore populations, one of which is not accessible to the quencher. The modified Stern-Volmer plots indicated that the fraction of accessible fluorophore (f_a) at the six positions was 0.8–0.9. The obtained Stern-Volmer constants of the accessible population ($K_{SV,a}$), presented in Table 2, indicated that the fluorophore is most exposed to solvent at pos. 94 and 140 and least exposed at pos. 22. However, the range of exposure among the sites was relatively small and there was no obvious relation between the $K_{SV,a}$ and *SA* values (Table 2).

EPR spectra of the IPSL- and MTSSL-labeled sTF mutants are shown as insets in Fig. 2, together with simulated lineshapes. The parameters obtained from the simulations are summarized in Table 3. All IPSL spectra show the three-line hyperfine pattern, associated with the isotropic hyperfine interaction between the unpaired electron and the nitrogen nucleus of the spin label, that is characteristic of fast spin label motion. The IPSL spectra could be simulated with a single motional component, which reported on rather high diffusion constants ($R_\perp$, $R_\parallel$) with large motional anisotropy ($R_\parallel/R_\perp \gg 1$). The rotational correlation time (ϕ_c), calculated from Eq. 1, reflects the motion of IPSL at the particular site of attachment. Its mobility was largest and most anisotropic when situated at pos. 94, and smallest at pos. 22, but the differences are quite small (Tables 3 and 4). For the spectra of the MTSSL-labeled sTF mutants, a second motional component was in some cases (pos. 94, 158, and 207) visible and, therefore, an additional component was used in the simulations. This indicates that MTSSL resides in two separate orientations with different local environment. The slowest of the two components was dominant for all three positions and the difference in ϕ_c between the two components was largest for pos. 207 (Table 4). MTSSL reported on the fastest motion at pos. 207, and the slowest at pos. 22, 158, and 207, but in general MTSSL was less mobile than IPSL. As in the case of IPSL, the motion of MTSSL was anisotropic, except for the slow spectral component at pos. 158 and 207, which was best-fitted with an isotropic component (Fig. 2, insets; Table 3).

The local environment of the different mutated sTF sites in the absence of FVIIa was also investigated with the fluorescent label IAEDANS. Intensity maxima were ob-

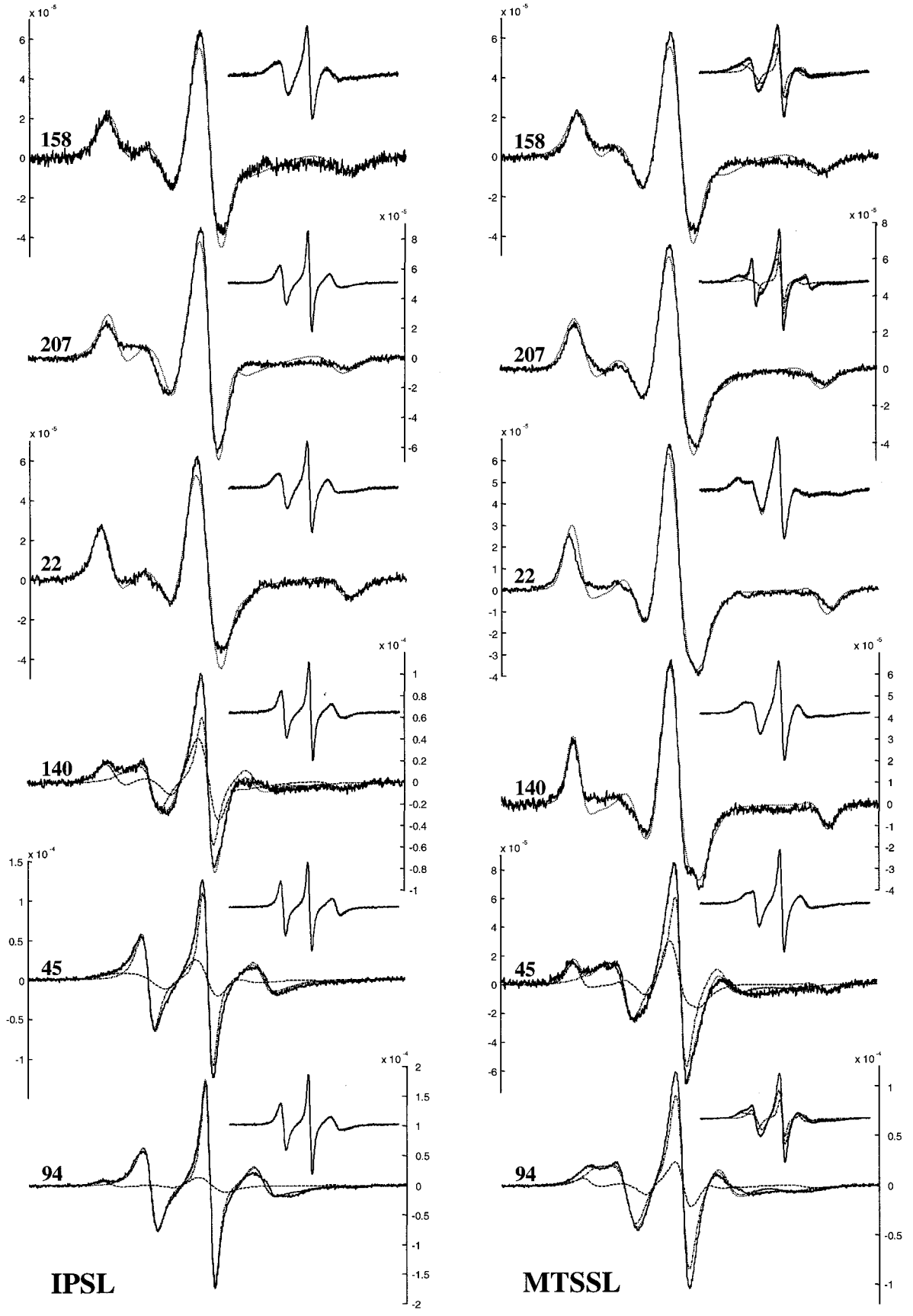
158
207
22
140
45
94
IPSL
MTSSL

served between 488 and 497 nm depending on position (data not shown) corresponding to IAEDANS in 20–45% ethanol (Owenius et al., 1999). Steady-state fluorescence anisotropy measurements were performed and the anisotropy of IAEDANS was found to be 0.07–0.11 (data not shown). Furthermore, fluorescence lifetime measurements were made, from which the IAEDANS lifetime was determined to be 12.6–15.5 ns (data not shown). Both parameters were used to calculate ϕ_c of IAEDANS at the various positions in sTF using the Perrin equation (Eq. 4). The low ϕ_c values (3.1–5.6 ns) indicated substantial local motion of IAEDANS at the surface-exposed sites (Table 4), being most pronounced at pos. 140 and smallest at pos. 22. Taken together, the data of the labeled sTF mutants indicate that the labels are solvent-exposed, thus sensing a rather polar environment, with moderate motional restrictions imposed by the surrounding residues.

Probing the binding interface between sTF and FVIIa

The sTF-Gla region

This region of the binding interface involves two of the selected sTF residues, W158 and V207. According to the crystal structure of sTF-FVIIa (Banner et al., 1996) the surface accessibility of the two residues are reduced to 5% and 0%, respectively, upon complex formation; i.e., they are more or less completely buried between the two interacting proteins. Fluorescence quenching of IAEDANS-labeled sTF-FVIIa indicated two populations, as in the absence of FVIIa. With IAEDANS at pos. 158 the modified Stern-Volmer plot indicated that the fraction of accessible fluorophore (f_a) was only 0.5. However, at pos. 207 and the remaining four positions, f_a for IAEDANS had a value similar (0.8–0.9) to its value in the absence of FVIIa. The degree of surface exposure of the IAEDANS fluorophore (i.e., the accessible fraction) was considerably decreased compared to that in sTF alone, concluded from the reduced $K_{SV,a}$ values of sTF-FVIIa (Table 2).

The EPR spectra of spin-labeled sTF-FVIIa describing the local environment of pos. 158 and 207 had similar lineshapes independent of the spin label used (Fig. 2). All four spectra were largely dominated by a broad spectral component, which has the features of a typical "powder spectrum" resulting from anisotropic hyperfine interaction. Such lineshapes are only obtained for spin labels involved in slow motion ($\phi_c > \sim 10$ ns). From single-component lineshape simulations of the spectra from spin-labeled sTF(W158C)-FVIIa, it was found that IPSL and MTSSL reported on ϕ_c values of 12 ns and 15 ns, respectively (Table 4). A similar analysis of the spectra from spin-labeled sTF(V207C)-FVIIa resulted in ϕ_c values of 12 ns (IPSL) or 29 ns (MTSSL). Thus, the motion probed by the spin labels was greatly reduced compared with that sensed at pos. 158 or 207 in the absence of FVIIa. Possible traces of a second, more mobile component were visible in some of the spectra, but they were too weak (of the same order of intensity as the uncertainty introduced by the Brownian diffusion model) to be simulated accurately, and were therefore neglected.

Substantial wavelength shifts were registered from the two IAEDANS-labeled sTF mutants upon association with FVIIa (Table 2). The blue-shift was 15 nm (→477 nm) and 30 nm (→465 nm) at pos. 158 and 207, respectively. This indicates that IAEDANS is in an environment corresponding to 75–100% ethanol in polarity (Owenius et al., 1999; Hammarström et al., 2001). The ϕ_c values obtained from the same samples were 14.9 ns at pos. 158 and 18.9 ns at pos. 207, i.e., four to five times longer compared to the times for IAEDANS-labeled sTF (Table 4). Taken together, the local environments of pos. 158, and especially pos. 207, became considerably more compact and less polar upon binding of FVIIa as reported by the labels.

The sTF-EGF1 region

Positions I22 and F140 are located in this contact region of sTF-FVIIa, and they are surface-exposed to 5% and 20% in the complex, respectively. The surface exposure of IAEDANS at the respective position, determined from the fluorescence quenching, was decreased compared with that in sTF alone; however, $K_{SV,a}$ decreased only from 3.4 M^{-1} to 2.4 M^{-1} at pos. 22 due to the relatively low exposure in the absence of FVIIa.

The EPR spectra of IPSL- or MTSSL-labeled sTF(I22C)-FVIIa have broad lineshapes similar to those found for the two sites in the sTF-Gla region (Fig. 2). The single-component simulations reported on ϕ_c values of 24 ns (IPSL) or 88 ns (MTSSL). Also, in the case of sTF(F140C)-FVIIa, MTSSL probed slow rotation (83 ns). However, the IPSL spectrum of sTF(F140C)-FVIIa was interpreted as a superposition of a slow ($\phi_c = 14$ ns) and a fast ($\phi_c = 1.4$ ns) component, the latter contributing with ~40%. The EPR data from simulations regarding pos. 140 (Table 3) differ slightly from those previously determined (Owenius et al., 1999), which were determined using an earlier version of

FIGURE 2 Experimental and simulated EPR spectra of (*left*) IPSL-labeled and (*right*) MTSSL-labeled sTF mutants in complex with FVIIa, and spectra of the same sTF variants in absence of FVIIa as insets. The different spectral components are: (——) experimental spectrum; (– – –) simulated c_1 or slow component if two-component spectrum; (–·–·–·) simulated c_2 or fast component if two-component spectrum; and (· · · · · ·) simulated spectrum. The parameters used in and obtained from the simulations are given in Table 3.

TABLE 4 Rotational correlation times calculated from dynamic parameters obtained from IAEDANS, IPSL, and MTSSL attached to different sTF mutants in the absence of and in complex with FVIIa

	ϕ_c (ns)								
	sTF				sTF-FVIIa				
			MTSSL‡			IPSL‡		MTSSL‡	
sTF Variant*	IAEDANS†	IPSL‡	c_1	c_2	IAEDANS†	Slow	Fast	Slow	Fast
W158C	3.4	1.0	6.4	1.5	14.9	12	—	15	—
V207C	3.6	0.9	6.7	0.4	18.9	12	—	29	—
I22C	5.6	1.3	6.9	—	12.6	24	—	88	—
F140C	3.1	1.0	2.5	—	15.7	14	1.4	83	—
W45C	5.2	1.0	3.4	—	11.6	5.4	0.8	83	1.0
Y94C	4.7	0.7	2.1	1.8	8.1	52	0.8	12	2.1

*W158 and V207 in the sTF-Gla region, I22 and F140 in the sTF-EGF1 region, and W45 and Y94 in the sTF-PD region.
†ϕ_c was determined from the Perrin equation (Eq. 4).
‡ϕ_c was determined from Eq. 1 using data in Table 3.

the simulation program lacking the least-squares analysis feature (Schneider and Freed, 1989).

A blue-shift of the emitted IAEDANS fluorescence was obtained also in this region upon complex formation with FVIIa, 5 nm at pos. 22 and 10 nm at pos. 140, and the polarity sensed by the probe was comparable to 40–50% ethanol (Owenius et al., 1999). The ϕ_c value at pos. 140, as reported by IAEDANS, was slightly higher than at pos. 22, but both were clearly increased compared to ϕ_c in free sTF (Table 4). The ϕ_c of IAEDANS at pos. 140 in sTF-FVIIa was lower than previously determined (Owenius et al., 1999), in which the fluorescence lifetime was estimated from the relative quantum yield instead of an actual lifetime measurement, and an average value of the factor *G* over the wavelength region was used.

In summary, the labels reported on slightly more apolar and considerably more rigid local environments of pos. 22 and 140 in the sTF-FVIIa complex compared to in sTF alone.

The sTF-PD region

This contact region contains the sTF residues W45 and Y94. These residues are exposed to 13% and 1%, respectively, in the crystal structure of the sTF-FVIIa complex. The fluorescence quenching measurements showed rather small decreases of the Stern-Volmer constant upon complex formation (Table 2).

The EPR spectra of IPSL- or MTSSL-labeled sTF-FVIIa presented rather complicated lineshapes indicating more than one spectral component (Fig. 2). It was necessary to apply two motional components to obtain good simulations. Using IPSL at pos. 45, there was clear evidence of local motion despite the presence of FVIIa, with a ϕ_c value that is similar to that of spin-labeled sTF(W45C) alone (Table 4). However, a broader component was also found (ϕ_c = 5.4 ns). Also, MTSSL reported on a mobile local component, but the slow component (ϕ_c = 83 ns) was more well defined than that of IPSL. For both labels the contribution from the slow component was ~50%. Similarly, the motion of both spin labels at pos. 94 in sTF-FVIIa was clearly influenced by a fast local component, with a somewhat higher ϕ_c value than in the absence of FVIIa. The slow component was rather pronounced in the spectra of both spin labels (IPSL: ϕ_c = 52 ns, MTSSL: ϕ_c = 12 ns), but contributed only with ~25% to the spectral intensity.

The fluorescence wavelength shift of IAEDANS upon complex formation was small (1–2 nm) at both pos. 45 and 94. The polarity of their surroundings was comparable to ~40% ethanol (Owenius et al., 1999). Also in this region of sTF-FVIIa, the ϕ_c values reported by IAEDANS were increased compared to those determined for free sTF (Table 4), and ϕ_c at pos. 45 was slightly higher than at pos. 94.

Conclusively, the labels reported on a minor decrease in polarity due to FVIIa binding and mixed motional states with substantial local motion at pos. 45 and 94 of the sTF-FVIIa interface.

DISCUSSION

Site-directed labeling techniques are currently used in numerous ways to obtain structural information about membrane proteins and high-molecular-weight proteins in solution, as well as in studies of protein folding and conformational transitions. In addition, this approach is applicable to the mapping of protein-protein interactions and conformational transitions upon protein association, as shown for human carbonic anhydrase II (HCAII) and the chaperonin GroEL (Persson et al., 1999; Hammarström et al., 2000), and in studies of protein aggregation (Hammarström et al., 1999). Recently, we used this approach on the receptor-ligand system sTF-FVIIa to obtain local information about the binding interface at a selected position (Owenius et al., 1999). The sTF-FVIIa complex is known to rely on very specific protein-protein interactions distributed

over an extensive contact surface, divided into three regions (Banner et al., 1996), and the significance of individual side chains is known from mutational studies (Gibbs et al., 1994; Ruf et al., 1994, 1995; Schullek et al., 1994; Kelley et al., 1995). However, these latter investigations are based on global methods, such as functional and binding assays, and SPR, i.e., the importance of a residue is judged from the effect of its removal on the cofactor function of sTF or on the overall binding of FVIIa to sTF. Further information about the two interacting proteins, but at a local level, can be obtained by studying the local environment of sTF residues along the sTF-FVIIa interface using the site-directed labeling approach.

In the present study we used the sTF-FVIIa complex as a model system of two interacting proteins to evaluate the application of specifically attached labels to investigate a binding surface at multiple sites. Six single-Cys mutants of sTF were made and each mutant was then labeled with sulfhydryl-specific spin and fluorescent labels. Spin labels are sensitive to the local compactness of the surrounding protein structure, which determines the mobility of the spin label and thereby the lineshape of the associated EPR spectrum. Lineshape simulations were performed to quantify the motion of the spin labels and thereby obtain more details of the local dynamic structure surrounding them. Fluorescent labels give information about the polarity of the environment in its vicinity, detected as a wavelength shift of the emitted light, but also the dynamics of the label was determined from fluorescence anisotropy and lifetime measurements. By monitoring the quenching of the fluorescence in the presence of acrylamide, the accessibility of the fluorophore was determined.

Local environments in sTF in the absence of FVIIa

The rather short ϕ_c values (3–6 ns) determined from anisotropy and lifetime data reported by the fluorescent label IAEDANS were expected from the large solvent exposure of the label (Table 2). Furthermore, the EPR spectra obtained from the IPSL-labeled sTF mutants showed that the label is in a state of intermediate mobility (Fig. 2, insets; Table 4). When ϕ_c^{local} is sufficiently short and $\phi_c^{local} \ll \phi_c^{global}$, the local motion of the label completely dominates the spectral lineshape. The large motional anisotropy, due to a faster axial rotation ($R_\parallel$), indicated that the neighboring residues put restrictions especially on the motion in the plane orthogonal to the parallel component ($R_\perp$). In general, the mobility of MTSSL is lower compared to that of IPSL at the different sites (Tables 3 and 4). An explanation for this behavior could be the lower flexibility of MTSSL compared to that of IPSL due to the disulfide linkage to the protein and the interaction of the disulfide bond with main-chain atoms (Mchaourab et al., 1996; Owenius et al., 1999; Langen et al., 2000). Thus, the motion of a protein-attached label is governed by the structural restrictions imposed by the surrounding protein structure, but also by the flexibility and physicochemical character of the label, which can promote interaction with nearby groups. Therefore, such a multitude of EPR lineshapes and ϕ_c values are observed for the selected sTF sites.

Global and local consequences of the introduced labels

By choosing sites in sTF that are important for binding FVIIa, the probability of detecting an environmental change upon FVIIa binding is increased. Unfortunately, this will also affect structural and functional properties of the sTF mutant. However, the introduction of a label was sometimes seen to improve the cofactor function of some sTF mutants, e.g., sTF(W158C) and sTF(V207C) (Table 1). Apparently, the introduced labels can use the cavity created by the mutation, even though the labels are too large to fit completely (Owenius et al., 1999), and at least in regions dominated by hydrophobic interactions they contribute to the binding capacity.

The different $K_{d(app)}$ values of different protein variants constitute a problem in the application of site-directed labeling to study protein-protein interactions, because difficulties are introduced in the data analysis and comparison of data between sites. The reduced binding affinity, which is a global parameter, is probably the direct consequence of the structural disturbance caused by the labeled Cys residue. It is therefore necessary to pay attention to the large differences in $K_{d(app)}$ among the differently labeled sTF mutants and take this into account in the analysis of spectroscopic data.

Local environments along the sTF-FVIIa interface

Upon association of sTF and FVIIa the wild-type residues in sTF selected for Cys mutation and labeling are exposed to the interacting part of FVIIa, and the degree of surface accessibility is reduced to between 0 and 20%. Because the structure of sTF is known not to change due to FVIIa association, any detectable spectral changes originate from the formation of the sTF-FVIIa complex.

The sTF-Gla region

Of the six labeled sTF mutants, sTF(W158C) and sTF(V207C) were those with the least functional perturbation due to the introduced labels, with $K_{d(app)}$ values only 1.9–6.5 times that of wt-sTF (Table 1). Therefore, we anticipate that the local structural perturbations in the vicinity of pos. 158 and 207 are small. For both IPSL- and MTSSL-labeled sTF-FVIIa the EPR spectra were dominated by the "powder" features of a slowly rotating spin

label (Fig. 2). The one-component lineshape simulations of the assumed global isotropic motion did not produce perfect fits (a known drawback of the Brownian diffusion model; Freed, 1976). If the shape of the sTF-FVIIa complex is modeled as a circular cylinder, the diffusion coefficients can be determined by hydrodynamic theory (Tirado and de la Torre, 1980; Keyes and Bobst, 1995). The cylinder dimensions were taken from Banner et al. (1996): length, 115 Å; radius, 22.5 Å. Assuming a temperature of 20°C and a viscosity of 0.001 Ns/m^2, the modeled diffusion coefficients became: $R_\perp = 1.6 \cdot 10^6\ s^{-1}$, $R_\parallel = 4.6 \cdot 10^6\ s^{-1}$, i.e., with some motional anisotropy ($R_\parallel/R_\perp \sim 3$), resulting in an average ϕ_c value of ~61 ns (Eq. 1). At these low diffusion rates (near the rigid limit) the sensitivity of the EPR spectrum to motional anisotropy is low, which means that the assumption of an isotropic global tumbling of the protein complex made in the simulations is legitimate. In comparison with the modeled diffusion, the simulations presented shorter ϕ_c values (Table 4) than the time expected from a spin label tightly locked within the protein structure, indicating minor local motion of the spin labels. The fluorescent label reported on ϕ_c values similar to the spin labels (Table 4), which in fact were two of the three longest times detected with IAEDANS. Both the fluorescence wavelength shifts (the two largest) and the Stern-Volmer constants (the two lowest) further emphasized that the environments at these two positions are the most apolar and least accessible of the studied sites (Table 2). In fact, IAEDANS reported on wavelengths, λ_{Fmax}(sTF-FVIIa), similar to values previously obtained from hydrophobic clusters of the globular protein HCAII (Svensson et al., 1995; Hammarström et al., 2001).

Thus, all labels are probably involved in minor local motion at their site of attachment (pos. 158 and 207) within the interface, but the dominating "powder" features of the EPR spectra from both spin labels and low emission wavelengths of IAEDANS point to structured hydrophobic local environments with high compactness. It seems like either W158 or V207 of the sTF-Gla region, both known to take major part in the regional hydrophobic interaction (Banner et al., 1996), can be substituted for another side chain without altering the compactness of the interface in this region. The minor importance of individual sTF residues in general in the sTF-Gla region, for the affinity of sTF for FVIIa, was previously demonstrated in a more global sense by SPR measurements (Kelley et al., 1995).

The sTF-EGF1 region

The two sTF mutants in this region, sTF(I22C) and sTF(F140C), were subjected to larger functional perturbations than sTF(W158C) and sTF(V207C) when introducing the labels ($K_{d(app)}$ values 10–55 times that of wt-sTF) (Table 1). Still, the ability of the labeled sTF(F140C) derivatives to activate FVIIa was previously found to be at least 75% of that of wt-sTF and their overall conformation seemed to be intact (Owenius et al., 1999; Österlund et al., 2000). The rather low, identical $K_{d(app)}$ values of MTSSL-labeled sTF(I22C) and sTF(F140C) imply that the MTSSL data obtained from the two positions are representative of the wt-sTF-EGF1 interface and can be compared with each other. Spectra of MTSSL-labeled sTF(I22C)-FVIIa and sTF(F140C)-FVIIa showed similar "powder" lineshapes to those seen in the sTF-Gla region (Fig. 2). However, the isotropic one-component simulations indicated even lower ϕ_c values (~85 ns, Table 4), i.e., of the order of the modeled tumbling of the protein complex itself (see above). Also for IPSL-labeled sTF(I22C)-FVIIa and sTF(F140C)-FVIIa, spectra were dominated by the slow global component, with similar (pos. 140) or higher (pos. 22) ϕ_c values compared to those of IPSL at pos. 158 and 207. The less compact structure in the vicinity of pos. 140 than around pos. 22 could be due to the more perturbed functional binding due to IPSL at pos. 140 (Table 1). At pos. 140, as previously shown (Owenius et al., 1999), a local component is also present in the spectrum, indicative of a rather mobile label, but less mobile than in the absence of FVIIa. The higher rotational freedom of IPSL compared to MTSSL at pos. 140 can be explained by their different properties (Mchaourab et al., 1996; Owenius et al., 1999; Langen et al., 2000). However, we cannot completely rule out the influence of the site-directed labeling on the local structure, possibly reflected upon by the much higher $K_{d(app)}$ of IPSL-labeled sTF(F140C) compared to that of MTSSL-labeled sTF(F140C) (Table 1). This makes EPR data from IPSL-labeled sTF(F140C)-FVIIa the least reliable as a description of the wild-type situation of all EPR data from the two positions. Fluorescence data from the IAEDANS-labeled sTF-FVIIa showed less solvent exposure, larger blue-shift, and higher ϕ_c of the label at pos. 140 in relation to pos. 22 (Tables 2 and 4). Taken together, their local environments were reported as slightly less (pos. 22) or similarly (pos. 140) compact, but not as apolar as those of the two sTF-Gla sites (pos. 158 and 207). The latter observation is likely due to the higher presence of vicinal polar residues and the larger solvent exposure of the fluorophore at pos. 22 and 140, although some influence from the lower binding affinities of IAEDANS-labeled sTF(I22C) and sTF(F140C) cannot be excluded. The ϕ_c values of IAEDANS (including those at pos. 158 and 207) are comparable to those of IPSL. This is indicative of some residual motion, possibly enabled by the more flexible structure of IAEDANS compared to that of MTSSL, and the lower binding affinities of the IAEDANS-labeled mutants compared to those of the MTSSL-labeled mutants.

Despite the weaker binding affinities of labeled sTF(I22C) and sTF(F140C) compared to those of labeled sTF(W158C) and sTF(V207C), all labels (with reservation for IPSL at pos. 140 due to its major perturbation) report on compact local environments. In fact, the rigidity of the

vicinal structures is large enough to tightly lock MTSSL within the binding interface at the two sites. The degree of immobilization of the spin labels at pos. 22, 140, 158, and 207 upon FVIIa binding, i.e., along a major part of the whole binding interface, is equal or even more pronounced compared to what previously has been observed when the labels are embedded in the hydrophobic interior of a protein (Lindgren et al., 1993; Svensson et al., 1995; Hammarström et al., 2001). This is indicative of interactions of similar strength as in the interior of a globular protein. A very similar packing density of atoms at recognition sites and protein interiors is seen for a large number of protein-protein complexes (Lo Conte et al., 1999). Both I22 and F140 contribute with major hydrophobic interactions with FVIIa (Banner et al., 1996). The compactness sensed in the vicinity of pos. 22 is probably maintained, despite its substitution, as a consequence of the strong FVIIa-binding contributions by the adjacent residues K20 and D58 (Kelley et al., 1995). K20 is especially important because it participates in both hydrophobic and hydrogen bonding interactions (Banner et al., 1996). F140 is in itself more important for FVIIa binding than I22 (Kelley et al., 1995), but is also supported by nearby sTF residues (e.g., R131, L133) engaged in hydrophobic interaction, however, with small individual binding contributions (Kelley et al., 1995; Banner et al., 1996). This probably maintains the compact environment at pos. 140 despite the modified side chain, at least if the label does not cause too much perturbation. The higher polarity probed by IAEDANS in the sTF-EGF1 region compared to that of the sTF-Gla region is likely the effect of the higher occurrence of polar residues in the sTF-EGF1 interface (Banner et al., 1996).

The sTF-PD region

The functional binding of the labeled variants of sTF(W45C) and sTF(Y94C) to FVIIa was largely perturbed ($K_{d(app)}$ values ~50–800 times that of wt-sTF) (Table 1). With very high $K_{d(app)}$ values, such as for IPSL-labeled sTF(W45C) and MTSSL-labeled sTF(Y94C), it is reasonable to assume that the local environment of the introduced label is somewhat altered from that of the wild-type residue. However, the amidolytic activities are still relatively high (IPSL-sTF(W45C) 85%, MTSSL-sTF(Y94C) 15%), indicating that native-like complexes are formed. Another consequence of very high $K_{d(app)}$ values is that unreasonably high protein concentrations are needed to form a stoichiometric complex. From the $K_{d(app)}$ values and protein concentrations used, the following percentages of formed sTF-FVIIa were expected: 78% (pos. 45, IPSL), 91% (pos. 45, MTSSL), 97% (pos. 94, IPSL), and 84% (pos. 94, MTSSL); i.e., there is a fraction of free spin-labeled sTF(W45C) and sTF(Y94C) in the samples. As shown in Fig. 2, all four EPR spectra of spin-labeled sTF(W45C)-FVIIa and sTF(Y94C)-FVIIa have features of two spectral components: one broad, corresponding to slow motion, and one narrow, emanating from a rapidly diffusing spin label. Table 3 shows that the diffusion tensor parameters ($R_\perp$, $R_\parallel$) of the fast component were similar to those of the spectrum in the absence of FVIIa, thus confirming the existence of uncomplexed sTF variants. However, according to the simulations, the fast component contributed with ~50% at pos. 45 and 74% at pos. 94, i.e., considerably more than expected. The additional contribution to the fast component probably has its origin in a second fraction of spin labels (different from the slow component) in a relatively unrestricted environment despite the presence of FVIIa, whose motion is undistinguishable from that of the spin label in free sTF.

The slow motional component found in all four spectra originates from a more restricted population of spin labels. In MTSSL-labeled sTF(W45C)-FVIIa it had a ϕ_c value (83 ns) comparable to the tumbling of the protein complex, i.e., in this orientation MTSSL becomes locked by the surrounding structure (Table 4). IPSL was much less restricted in sTF(W45C)-FVIIa, which is likely due to the larger (>3×) perturbation caused by IPSL and its different properties compared to MTSSL. On the contrary, when sTF-FVIIa was probed at pos. 94, the slow-mobility component of the IPSL spectrum corresponded to a highly immobilized label (almost completely locked; ϕ_c = 52 ns), whereas MTSSL was slightly less restricted at the same site (ϕ_c = 12 ns). This is probably due to the >12× lower $K_{d(app)}$ value of IPSL-labeled sTF(Y94C). However, the unexpectedly small difference in ϕ_c could possibly be due to the lower flexibility of MTSSL compared to IPSL. Because the $K_{d(app)}$ values of the IAEDANS-labeled sTF mutants in the sTF-PD region were only somewhat larger than those of IPSL-labeled sTF(Y94C), but not as large as those of MTSSL-labeled sTF(W45C), IAEDANS can provide additional information about the two sites. Indications of a less structured local environment were found from the surface exposure of the IAEDANS fluorophore (largest of the six studied sites) and the fluorescence blue-shift (smallest of the six studied sites) (Table 2). The rather polar environments of pos. 45 and 94 in sTF-FVIIa, comparable to those of pos. 22 and 140, are likely a consequence of the vicinal polar residues and the relatively high accessibility of the fluorophore. The effect of the quite low binding affinities of the IAEDANS-labeled sTF(W45C) and sTF(Y94C) on the accessibility cannot be excluded (Table 1). The short ϕ_c values provided further evidence for a considerable local flexibility of the label at both sites.

To conclude, both W45 and Y94 are important for binding of FVIIa and the binding interface in this region is rather complex, with both residues directly involved in three of the five identified key interactions (Kelley et al., 1995; Banner et al., 1996). The existence of a local motional component with fast dynamics in the EPR spectra and the large degree of exposure and flexibility of the fluorescent label suggest that the global perturbation of the labels may be a direct

consequence of the somewhat perturbed local structure that is probed by the labels. However, the co-existence of a slow-motional component, particularly in the EPR spectra of the least perturbed spin-labeled sTF-FVIIa variants in this region, suggests that there might be a tight binding interface, perhaps similar to the other two regions, also in the sTF-PD region in the native situation.

CONCLUSIONS

In the present study we have probed the protein-protein interaction between sTF and FVIIa and investigated the extended binding interface at multiple sites by introducing spin and fluorescent labels that are sensitive to their local environment. We have brought attention to the problems induced by the different $K_{d(app)}$ values of the labeled sTF mutants, such as what effects this has on the reliability of the spectroscopic data and how this influences the comparison of data from various labels and positions. By using the multi-probing strategy the probability of obtaining complementary native-like information about the contact surface of sTF-FVIIa at multiple sites was increased and the risk of misinterpretation of data was reduced. We find that pos. 22 and 140 in the sTF-EGF1 region, and pos. 158 and 207 in the sTF-Gla region, are situated in structurally very compact environments, indicative of strong binding contributions from hydrophobic interactions. The compactness detected by all labels at the four sites and the apolarity detected by the fluorescent label at pos. 158 and 207 are equal to or even more pronounced than in the rigid hydrophobic core of a globular protein. It is difficult to make reliable conclusions about the interface of the sTF-PD region because the binding of labeled sTF(W45C) and sTF(Y94C) is so perturbed. Not surprisingly, the labels report on polar unstructured environments, but interestingly, we also find indications of a rigid contact surface in this region that might be representative of the wild-type complex. The results of the present study suggest that complementary data from spin and fluorescent labels enable 1) the comparison of the tightness of interaction, and 2) the distinction between regions with different amino acid and interaction characteristics locally along a protein-protein binding interface.

R.O. and M.Ö. are Ph.D. students at the graduate school Forum Scientum, which is funded by the Swedish Foundation for Strategic Research. This work was also supported by grants from the Swedish Medical Research Council (to U.C. and M.S.) and the Swedish Natural Science Research Council (to U.C.).

REFERENCES

Banner, D. W., A. D'Arcy, C. Chène, F. K. Winkler, A. Guha, W. H. Konigsberg, Y. Nemerson, and D. Kirchhofer. 1996. The crystal structure of the complex of blood coagulation factor VIIa with soluble tissue factor. *Nature.* 380:41–46.

Berliner, L. J., and J. Reuben, editors. 1989. Biological Magnetic Resonance, Vol. 8. Spin Labeling—Theory and Applications. Plenum Press, New York.

Budil, D. E., S. Lee, S. Saxena, and J. H. Freed. 1996. Nonlinear-least-squares analysis of slow-motion EPR spectra in one and two dimensions using a modified Levenberg-Marquardt algorithm. *J. Magn. Reson.* 120:155–189.

Carlsson, U., and B.-H. Jonsson. 1995. Folding of β-sheet proteins. *Curr. Opin. Struct. Biol.* 5:482–487.

Feix, J. B., and C. S. Klug. 1998. Site-directed spin labeling of membrane proteins and peptide-membrane interactions. *In* Biological Magnetic Resonance, Vol. 14. Spin Labeling: The Next Millenium. L. J. Berliner, editor. Plenum Press, New York. 251–281.

Freed, J. H. 1976. Theory of slow tumbling ESR spectra for nitroxides. *In* Spin Labeling: Theory and Applications, Vol. 1. L. J. Berliner, editor. Academic Press, New York. 53–132.

Freskgård, P.-O., O. H. Olsen, and E. Persson. 1996. Structural changes in factor VIIa induced by Ca^{2+} and tissue factor studied using circular dichroism spectroscopy. *Protein Sci.* 5:1531–1540.

Gibbs, C. S., S. N. McCurdy, L. L. K. Leung, and L. R. Paborsky. 1994. Identification of the factor VIIa binding site on tissue factor by homologous loop swap and alanine scanning mutagenesis. *Biochemistry.* 33: 14003–14010.

Goldman, S. A., G. V. Bruno, and J. H. Freed. 1972. Estimating slow-motional rotational times for nitroxides by electron spin resonance. *J. Phys. Chem.* 76:1858–1860.

Hammarström, P., R. Owenius, L.-G. Mårtensson, U. Carlsson, and M. Lindgren. 2001. High resolution probing of local conformational changes in proteins by the use of multiple labeling. Unfolding and self assembly of human carbonic anhydrase II monitored by spin, fluorescent, and chemical reactivity probes. *Biophys. J.* 80:2867–2885.

Hammarström, P., M. Persson, P.-O. Freskgård, L.-G. Mårtensson, D. Andersson, B.-H. Jonsson, and U. Carlsson. 1999. Structural mapping of an aggregation nucleation site in a molten globule intermediate. *J. Biol. Chem.* 274:32897–32903.

Hammarström, P., M. Persson, R. Owenius, M. Lindgren, and U. Carlsson. 2000. Protein substrate binding induces conformational changes in the chaperonin GroEL. A suggested mechanism for unfoldase activity. *J. Biol. Chem.* 275:22832–22838.

Harlos, K., D. M. A. Martin, D. P. O'Brien, E. Y. Jones, D. I. Stuart, I. Polikarpov, A. Miller, E. G. D. Tuddenham, and C. W. G. Boys. 1994. Crystal structure of the extracellular region of human tissue factor. *Nature.* 370:662–666.

Hubbell, W. L., D. S. Cafiso, and C. Altenbach. 2000. Identifying conformational changes with site-directed spin labeling. *Nature Struct. Biol.* 7:735–739.

Hubbell, W. L., A. Gross, R. Langen, and M. A. Lietzow. 1998. Recent advances in site-directed spin labeling of proteins. *Curr. Opin. Struct. Biol.* 8:649–656.

Hubbell, W. L., H. S. Mchaourab, C. Altenbach, and M. A. Lietzow. 1996. Watching proteins move using site-directed spin labeling. *Structure.* 4:779–783.

Kelley, R. F., K. E. Costas, M. P. O'Connell, and R. A. Lazarus. 1995. Analysis of the factor VIIa binding site on human tissue factor: effects of tissue factor mutations on the kinetics and thermodynamics of binding. *Biochemistry.* 34:10383–10392.

Keyes, R. S., and A. M. Bobst. 1995. Detection of internal and overall dynamics of a two-atom-tethered spin-labeled DNA. *Biochemistry.* 34: 9265–9276.

Krinichnyi, V. I., O. Y. Grinberg, V. R. Bogatyrenko, G. I. Likhtenshtein, and Y. S. Lebedev. 1985. Study of the influence of the microsurroundings on magneto-resonance parameters of spin-labeled human serum albumin in the 2 mm ESR range. *Biophysics.* 30:233–237.

Lakowicz, J. R. 1999. Principles of Fluorescence Spectroscopy. 2nd Ed. Kluwer Academic/Plenum Publishers, New York.

Langen, R., K. J. Oh, D. Cascio, and W. L. Hubbell. 2000. Crystal structures of spin labeled T4 lysozyme mutants: implications for the interpretation of EPR spectra in terms of structure. *Biochemistry.* 39: 8396–8405.

Likhtenshtein, G. I. 1993. Biophysical Labeling Methods in Molecular Biology. Cambridge University Press, New York.

Lindgren, M., M. Svensson, P.-O. Freskgård, U. Carlsson, B.-H. Jonsson, L.-G. Mårtensson, and P. Jonasson. 1993. Probing local mobility in carbonic anhydrase: EPR of spin-labeled SH groups introduced by site-directed mutagenesis. *J. Chem. Soc., Perkin Trans.* 2:2003–2008.

Lo Conte, L., C. Chothia, and J. Janin. 1999. The atomic structure of protein-protein recognition sites. *J. Mol. Biol.* 285:2177–2198.

Mchaourab, H. S., M. A. Lietzow, K. Hideg, and W. L. Hubbell. 1996. Motion of spin-labeled side chains in T4 lysozyme. Correlation with protein structure and dynamics. *Biochemistry.* 35:7692–7704.

Muller, Y. A., M. H. Ultsch, and A. M. d. Vos. 1996. The crystal structure of the extracellular domain of human tissue factor refined to 1.7 Å resolution. *J. Mol. Biol.* 256:144–159.

Muller, Y. A., M. H. Ultsch, R. F. Kelley, and A. M. d. Vos. 1994. Structure of the extracellular domain of human tissue factor: location of the factor VIIa binding site. *Biochemistry.* 33:10864–10870.

Ondar, M. A., O. Y. Grinberg, A. A. Dubinskii, and Y. S. Lebedev. 1985. Study of the effect of the medium on the magnetic-resonance parameters of nitroxyl radicals by high-resolution EPR spectroscopy. *Sov. J. Chem. Phys.* 3:781–792.

Österlund, M., R. Owenius, E. Persson, M. Lindgren, U. Carlsson, P.-O. Freskgård, and M. Svensson. 2000. Spectroscopic probing of the influence of calcium and the Gla domain on the interaction between the first EGF domain in factor VIIa and tissue factor. *Eur. J. Biochem.* 267: 6204–6211.

Owenius, R., M. Österlund, M. Lindgren, M. Svensson, O. H. Olsen, E. Persson, P.-O. Freskgård, and U. Carlsson. 1999. Properties of spin and fluorescent labels at a receptor-ligand interface. *Biophys. J.* 77: 2237–2250.

Persson, M., P. Hammarström, M. Lindgren, B.-H. Jonsson, M. Svensson, and U. Carlsson. 1999. EPR mapping of interactions between spin-labeled variants of human carbonic anhydrase II and GroEL: evidence for increased flexibility of the hydrophobic core by the interaction. *Biochemistry.* 38:432–441.

Persson, E., O. H. Olsen, A. Østergaard, and L. S. Nielsen. 1997. Ca^{2+} binding to the first epidermal growth factor-like domain of factor VIIa increases amidolytic activity and tissue factor affinity. *J. Biol. Chem.* 272:19919–19924.

Ruf, W., C. R. Kelly, J. R. Schullek, D. M. A. Martin, I. Polikarpov, C. W. G. Boys, E. G. D. Tuddenham, and T. S. Edgington. 1995. Energetic contributions and topographical organization of ligand binding residues of tissue factor. *Biochemistry.* 34:6310–6315.

Ruf, W., J. R. Schullek, M. J. Stone, and T. S. Edgington. 1994. Mutational mapping of functional residues in tissue factor: identification of factor VII determinants in both structural modules of the predicted cytokine receptor homology domain. *Biochemistry.* 33:1565–1572.

Schneider, D. J., and J. H. Freed. 1989. Calculating slow motional magnetic resonance spectra. *In* Biological Magnetic Resonance, Vol. 8. Spin Labeling—Theory and Applications. L. J. Berliner and J. Reuben, editors. Plenum Press, New York. 1–76.

Schullek, J. R., W. Ruf, and T. S. Edgington. 1994. Key ligand interface residues in tissue factor contribute independently to factor VIIa binding. *J. Biol. Chem.* 269:19399–19403.

Svensson, M., P. Jonasson, P.-O. Freskgård, B.-H. Jonsson, M. Lindgren, L.-G. Mårtensson, M. Gentile, K. Borén, and U. Carlsson. 1995. Mapping the folding intermediate of human carbonic anhydrase II. Probing substructure by chemical reactivity and spin and fluorescence labeling of engineered cysteine residues. *Biochemistry.* 34:8606–8620.

Thim, L., S. Bjoern, M. Christensen, E. M. Nicolaisen, T. Lund-Hansen, A. H. Pedersen, and U. Hedner. 1988. Amino acid sequence and post-translational modifications of human factor VIIa from plasma and transfected baby hamster kidney cells. *Biochemistry.* 27:7785–7793.

Tirado, M. M., and J. G. de la Torre. 1980. Rotational dynamics of rigid, symmetric top macromolecules. Application to circular cylinders. *J. Chem. Phys.* 73:1986–1993.